JCTC Journal of Chemical Theory and Computation

A Molecular Dynamics Simulation of the Binding Modes of D-Glutamate and D-Glutamine to Glutamate Racemase

Eduard Puig,[†] Mireia Garcia-Viloca,[‡] Àngels González-Lafont,[†,‡] Inés López,[‡] Xavier Daura,[‡,§] and José M. Lluch*[,†,‡]

Departament de Química and Institut de Biotecnologia i de Biomedicina, Universitat Autònoma de Barcelona, 08193 Bellaterra, Barcelona, Spain, and Institució Catalana de Recerca i Estudis Avançats (ICREA), 08010 Barcelona, Spain

Received November 19, 2004

Abstract: Classical molecular dynamics simulations of the D-Gln/*Aquifex pyrophilus* MurI and D-Glu/*Aquifex* pyrophilus MurI complexes have been carried out. Since the active site of the enzyme contains many charged and polar residues, several binding modes are possible. Thus, three very different stable conformations of the substrate analogue D-Gln have been found, and at least three binding modes are possible for the substrate D-Glu. These qualitative results give an explanation for the apparent disagreement between the D-Gln bound MurI X-ray crystal structure and the expected position and orientation of the substrate D-Glu in order to make it possible the assumed Cα deprotonation (by Cys70)/reprotonation (by Cys178) racemization mechanism.

Introduction

D-Amino acids are essential components of peptidoglycans (alternatively, mureins), which are the rigidifying components of the bacterial cell walls and protect the organism from osmotic lysis.[1] In particular, D-glutamate is a required biosynthetic building block added by the enzyme MurD ligase to the peptidoglycan intermediate uridine 5′-diphosphate-*N*-acetylmuramyl-L-alanine.[2,3] The enzyme glutamate racemase (MurI, EC 5.1.1.3) catalyzes the interconversion of glutamate enantiomers in a cofactor-independent fashion and provides bacteria with a source of D-glutamate.[1,4] Mutagenesis knockout experiments in *Streptococcus pneumoniae* (one of the most frequent causes of bacterial respiratory infection and meningitis) have shown that glutamate racemase is essential for the viability of this bacteria.[5] Thus, inhibition of glutamate racemase is a very attractive target for the design of new antibacterial agents,[6,7] specially taking into account the alarming increase in antimicrobial resistance.[8,9]

* Corresponding author phone: 34 93 581 2138; fax: 34 93 581 2920; e-mail: lluch@klingon.uab.es.

[†] Departament de Química, Universitat Autònoma de Barcelona.

[‡] Institut de Biotecnologia i de Biomedicina, Universitat Autònoma de Barcelona.

[§] Institució Catalana de Recerca i Estudis Avançats (ICREA).

Glutamate racemase, as all known amino acid racemases, seems to operate via an initial deprotonation of the amino acid's α-proton, followed by a reprotonation on the opposite face of the resulting planar anionic intermediate.[10,11] Mutagenesis studies support the idea that two cysteines are the catalytic acid/base residues. These two cysteine residues and surrounding residues are strictly conserved among all MurI and other cofactor-independent racemases, including aspartate racemase.[12] In the *Lactobacillus fermenti* glutamate racemase enzyme only two cysteine residues (Cys73 and Cys184) are present, and mutation of either of them to alanine eliminates the racemase activity.[13] Similar results were obtained with Cys-to-Thr/Ala mutants of the *Escherichia coli* enzyme.[14,15] In addition, Tanner et al. have used an irreversible inhibitor, aziridino-glutamate,[16] to show that at least one of the cysteines is in the proper vicinity to the α-carbon of the bound glutamate. Further studies by Glavas and Tanner[4,17,18] have determined that Cys73 is responsible for the deprotonation of the Cα atom of D-glutamate, whereas Cys184 is responsible for the reprotonation of the Cα atom of L-glutamate.

Recently, the X-ray crystallographic structure of glutamate racemase from *Aquifex pyrophilus* has been solved by Hwang et al.[19] at 2.3 Å resolution for both apo-MurI and MurI complexed with a substrate analogue, D-glutamine. The

10.1021/ct049881g CCC: $30.25
Published on Web 05/24/2005

corresponding coordinates have been deposited in the Protein Data Bank (PDB) with the accession codes 1b73 and 1b74, respectively. To our knowledge, apart from the case of the diaminopimelate epimerase,[20−22] no other structures of a cofactor-independent amino acid racemase are nowadays available. In this crystal, MurI exists as a tightly associated dimer, and the two monomers are related by a crystallographic 2-fold symmetry axis. Each monomer consists of two compact domains with α/β structure. A large groove is formed between the two domains. The dominant feature of the dimerization is an insertion of a loop and a α-helical region of one monomer into the large groove between the two domains in the other monomer. This way a deep pocket comprising residues from both monomers is formed in the region of the large groove.

In *Aquifex pyrophilus* the two catalytic cysteines are Cys70 and Cys178. The binding site of the inhibitor D-Gln has been observed to be in the deep pocket formed by the two monomers. A root-mean-square deviation (rmsd) of just 0.72 Å between apo- and D-Gln bound MurI structures indicates that the binding of D-Gln to MurI does not induce any important conformational changes. Surprisingly, while the Cδ atom of D-Gln has been found by Hwang et al.[19] to be sandwiched by the two thiol groups of Cys70 (5.1 Å) and Cys178 (3.0 Å), the Cα atom is more than 5.3−7.6 Å away from the two catalytic cysteines. Thus, in the active site D-Gln appears to be flipped 180° from the expected binding of the substrate D-Glu, in such a way that the Cδ and Cγ atoms of D-Gln occupy the positions of the Cα and Cβ atoms of D-Glu, respectively. Despite these results, Hwang et al.[19] have proposed, from mutagenesis studies, a Cα atom deprotonation (by Cys70)/reprotonation (by Cys178) mechanism for the racemization of D-Glu by MurI, in agreement with the mechanism suggested by Glavas and Tanner.[17,18] On the other hand, we have to point out[23] that the 1b74 structure deposited in the PDB is not the real crystal structure obtained by Hwang et al.[19] for the D-Gln Mur I complex but a theoretical model (described in ref 19). In this model the D-Gln coordinates were twisted 180° in order to be compatible with the Tanner's mechanism. This fact can be easily verified by analysis of the interatomic distances in the 1b74 structure, specially the Cα−Cys70 and Cα−Cys178 distances. To our knowledge this is still the situation at the moment of writing this paper.

Since the crystal structure actually determined by Hwang et al.[19] does not appear to be consistent with the assumed catalytic mechanism, several scenarios can be envisaged: (a) the binding mode of D-Glu is different from that of D-Gln; (b) the crystallographic model for the binding of D-Gln to Aquifex pyrophilus MurI does not correspond to the predominant binding mode in solution; and (c) racemization of the substrate D-Glu by MurI does not take place through the Cα atom deprotonation/reprotonation mechanism being the two cysteines the acid/base residues. Since experimental determination of the substrate D-Glu bound MurI crystal structure has not been done, a theoretical analysis of scenarios (a) and (b) can shed light on this question. To this aim, we present here classical molecular dynamics simulations of the D-Gln/Aquifex pyrophilus MurI and D-Glu/Aquifex pyrophilus MurI complexes. Our structural results will provide an adequate starting point for later reactivity studies.

Methods

Models of the Enzyme−Ligand Complex. In the present study, a total of 6 models have been used to computationally determine the possible orientations of the inhibitor D-Gln and the substrate D-Glu in the active site of MurI. The D-Gln-X-ray model is based on the Cartesian coordinates actually determined by X-ray crystallography, which were kindly given to us by Hwang, Cho, and co-workers. The D-Gln-modeled model is based on the Cartesian coordinates contained in the Protein Data Bank at the moment of writing this paper (code 1b74). These two sets of coordinates only differ in the ligand coordinates. The 1b73 file (containing the coordinates of the ligand-free enzyme) has been used to start the docking simulation explained below, and the results of this simulation have provided the initial structure for the D-Gln-docked model. In the case of the three models used to represent the D-Glu/*Aquifex pyrophilus* MurI complex, the starting Cartesian coordinates are the same sets of coordinates cited above but replacing the D-Gln ligand by a D-Glu molecule or using a D-Glu molecule as the ligand in the docking simulation.

In all 6 models the coordinates of the hydrogen atoms of the ligand, the protein, and the crystallographic waters were determined using the HBUILD facility in the program CHARMM (Chemistry at HARvard Macromolecular Mechanics).[24] According to the mutagenesis studies by Glavas and Tanner[17] and Hwang et al.,[19] the strictly conserved residues Asp7 (Asp10 in *L. fermenti*), His180 (His186), and Glu147 (Glu152) have an important catalytic role in either stabilizing the carbanionic intermediate by hydrogen bonding interactions or assisting the cysteine bases in the deprotonation of glutamate. In addition, Glavas and Tanner[17] have also suggested that Glu147 (Glu152) play a role in glutamate binding.

Since the aim of this paper is to discern if the actual crystal structure determined by Hwang et al.[19] is compatible with Tanner's mechanism, we have assumed that Asp7, Glu147, and His180 are protonated in the active site of MurI at neutral pH. On the other hand, we have deprotonated the catalytic Cys70 residue to be consistent with its proposed role as the base that abstracts the α-proton in the D to L direction of the racemase reaction. Thus, the active site protonation state assumed to be coherent with the proposed mechanism shows a deprotonated Cys70 close to a protonated Asp7. The measured kinetic isotope effects suggest that Asp7 could assist Cys70 either by hydrogen bonding to the thiolate or by deprotonating the thiol.[17] To check which of these two situations is more favorable, or in other words, which of the two residues would be preferentially protonated, two energy minimizations have been done. The first one corresponding to the state with Asp7 protonated and Cys70 deprotonated and the second one with Asp7 deprotonated and Cys70 protonated. The minimizations have been carried out on a 24 Å sphere around the substrate's Cα atom with a gradient tolerance of 0.001 kcal/molÅ, applying a nonbonded cutoff of 13 Å, and a switch function from 12 to 13 Å. The

solvation interactions have been modeled with one of the most accurate analytic Generalized Born approaches, the GB-MV2[25] method (the parameters used for this method are listed in the Supporting Information, Table 1) implemented in CHARMM c31.[24] It has to be noted that the GB-MV2 model is one of the most accurate analytic GB formalisms designed to mimic the standard molecular volume based Poisson−Boltzmann solvation energies.[24] We have found that the model with Cys70 deprotonated/Asp7 protonated is 2.5 kcal/mol more stable than the Cys70 protonated/Asp7 deprotonated model in terms of Gibbs free energy, thus confirming that the reactive model assumed in the present work is plausible. The protonation states for all other ionizable residues were set according to standard pK_a values and a pH of 7. Histidine residues were modeled as neutral or protonated, with the proton on Nϵ or/and Nδ, on the basis of possible hydrogen bond interactions in the X-ray crystallographic structure. The ligand was modeled in its amino acid zwitterionic form, that is, with the amino group protonated and the carboxylic group deprotonated.

In all 6 models, to mimic the aqueous environment, we used the stochastic boundary molecular dynamics (SBMD)[26,27] simulation technique by adding a 24 Å sphere of preequilibrated waters centered on the Cα atom of the substrate. Crystallographic water molecules beyond 24 Å of the origin of this sphere were removed. Water molecules with their oxygen atom at a distance of 2.5 Å or less from any non-hydrogen protein, ligand, or crystallographic water atom were also deleted. This procedure was repeated three times with randomly rotated water spheres. Then, a molecular dynamics simulation (5 ps) was carried out to relax energetically bad contacts, and the 3-fold cycle of superposition, rotation, and deletion was repeated to fill in additional cavities generated from the equilibration calculations. The final 6 models have slightly different total number of atoms comprised between 10 600 and 10 677. This resulting configurations are called "initial" in this paper.

In all the simulations, the protein and ligand atoms were modeled with the CHARMM22[28] force field, and the TIP3P[29] model was used for water. We note that in CHARMM22 only the protonated form of cysteine is an standard residue, and thus, we have used molecular mechanics parameters for a deprotonated cysteine residue extracted from the CHARMM22 standard parameters of ethylthiolate (see Supporting Information, Figure 1 and Tables 2−4).

Molecular Dynamics Simulations. The SBMD technique is an efficient approach to carry out molecular dynamics simulations of a region of the enzymatic system called the reaction zone. It reduces the total number of atoms that must be included in the simulation of the solvated system and, hence, minimizes the computational costs. The rest of the system or reservoir zone is held fixed during the simulations and provides a static field that supplies important electrostatic interactions of protein atoms near the reaction zone-reservoir zone boundary. In the present study, the reaction zone contains the active site residues and all protein and solvent atoms within a sphere of 24 Å centered on the C_α atom of the substrate. The reaction zone is further divided into the molecular dynamics region (containing the ligand, the enzymatic residues, and the water molecules within 20 Å of the center of the sphere), which is treated with Newtonian molecular dynamics, and the buffer region (from 20 to 24 Å), which represents a simplified heat bath and is treated by Langevin dynamics. For each ligand-MurI model, protein atoms were assigned to one or another region according to a reference structure at the beginning of the simulation and they retained their labels throughout the simulation, whereas water molecules were allowed to diffuse between the molecular dynamics region and the buffer region. The Langevin dynamics regime imposes a friction coefficient and a random force on the heavy atoms in the buffer region. These atoms are further restrained by imposing a harmonic restoring force to keep them close to their average positions and to help to maintain the structural integrity of the enzyme. The harmonic force constants were taken as 1.22 kcal mol^{-1} Å^{-2} for the main-chain O atoms, 1.30 kcal mol^{-1} Å^{-2} for all other main-chain atoms, and 0.73 kcal mol^{-1} Å^{-2} for side-chain atoms and atoms of water molecules. The friction constants were 200 ps^{-1} for the protein atoms and 62 ps^{-1} for the water atoms in the buffer region. A deformable boundary potential was imposed on water molecules at the buffer/reservoir interface to represent the effect of bulk solvent outside this boundary.

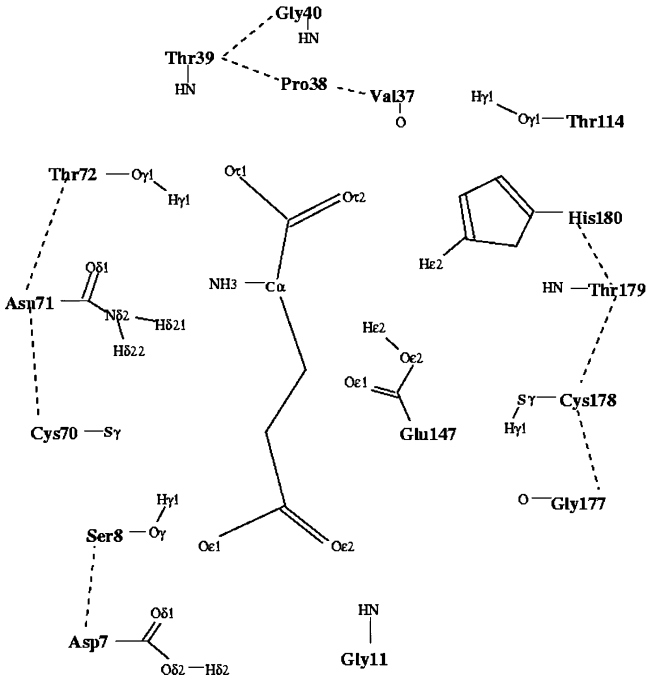

Figure 1. Schematic representation of the active site of MurI from *Aquifex pyrophilus* with a substrate molecule (glutamate) bounded. The labels on the atoms of the substrate and the enzymatic residues are the ones used in the tables.

To test the possible existence of larger-scale effects of the protein on the active site, we have repeated a SBMD simulation with a sphere of 30 Å to define the reaction zone. The results corresponding to the D-Glu-modeled system (see Supporting Information, Figure 2 and Table 5) show that, although some particular MurI−substrate interactions change, most of them are maintained. The essential trends of the relative orientation of the substrate are not modified when the reaction zone is enlarged from 24 to 30 Å.

We used an integration time step of 1 fs during the heating and equilibration simulations described below along with a nonbonded cutoff of 13 Å based on the center-of-mass separation between interacting groups. A switch function was added in the region from 12 to 13 Å to feather the interaction energy to zero. The nonbonded pair list was updated every 35 steps, which is suitable in a rather rigid system as an enzyme's active site. All bond lengths involving hydrogen atoms were constrained by the SHAKE algorithm,[30] and the relative dielectric permittivity was set to 1. Initially, we carried out 30 ps of SBMD simulations to heat the system up to 300 K and then 100 ps more to equilibrate it at this temperature. From the final structure we ran simulations for at least 1 ns, saving the generated structures at every 200 steps. These data were used for later structural analysis.

Docking Method. As mentioned above, the dimer was built from the monomer coordinates contained in PDB-entry 1b73. All crystallographic water molecules were removed. Initial models for D-Gln and D-Glu were generated from standard geometries. The AutoDock Tools[31] were used to add polar hydrogen atoms and to assign Kollman united-atom partial charges,[32,33] atomic solvation parameters,[32,33] and fragmental volumes.[32,33] The grid maps were calculated using AutoGrid 3.0,[33] with $61 \times 61 \times 61$ points and a grid-point spacing of 0.375 Å. The maps were centered at the midpoint between the sulfur atoms of Cys70 and Cys178 (active site).

Ten docking runs were performed for each ligand using the Lamarckian Genetic Algorithm implemented in AutoDock 3.0,[33] which combines a genetic algorithm and an adaptative local-search algorithm. All torsional bonds of the ligand were allowed to rotate during the docking process. The step size was 0.2 Å for translations and 5° for orientations and torsions. These step sizes determine the relative size of mutation in the local search. The Cauchy distribution parameters α and β, determining the size of the mutation in the genetic algorithm, were set to 0 and 1, respectively.

The parameters for the genetic algorithm were set as follows: an initial population of 50 random individuals, a maximum of 1.5×10^6 energy evaluations, a maximum of 27 000 generations, an elitism value of 1 (number of top individuals that automatically survive into the next generation), a mutation rate of 0.02 (probability that a gene undergoes a random change), and a crossover rate of 0.80 (probability that two individuals undergo crossover). Proportional selection was used, where the average of the worst energy was calculated over a window encompassing the previous 10 generations. The pseudo-Solis and Wets local-search algorithm were chosen, with the following parameter settings: a maximum of 300 iterations per local search, a probability of 0.06 of performing local search on an individual in the population, a maximum of 4 consecutive successes or failures before doubling or halving, respectively, the local-search step size (ρ), and a lower bound on ρ (termination criterion for the local search) of 0.01.

Results and Discussion

Binding of D-Gln in the Active Site of MurI. Three models have been built to represent the D-Gln/*Aquifex pyrophilus* MurI complex, which only differ in the orientation of the ligand in the active site. The crystal structure files used to build these models contain the Cartesian coordinates for the enzyme atoms of the monomer contained in the crystallographic asymmetric unit (253 enzymatic residues) with one or no D-Gln molecule bound and 104 to 107 crystallographic waters. However, in the crystal, MurI exists as a tightly associated dimer, and the active site of each monomer in the dimer contains residues from the other monomer (for example, Glu147). On the basis of this crystallographic result Hwang et al.[19] proposed that dimerization is important for the racemase function and stability of *Aquifex pyrophilus* MurI. Thus, we have assumed that the dimer is the active form of MurI. A complete multimer, which corresponds to the known biologically significant oligomerization state of the molecule, has been generated by applying the operations of symmetry of the space group P6522, and from this structure we have trimmed a dimer.

The first model, the so-called D-Gln-X-ray model, is based on the ligand and enzyme Cartesian coordinates obtained by X-ray crystallography, whereas in the D-Gln-modeled model we have taken as relative orientation of the ligand in the active site the one modeled by Hwang et al.[19] on the basis of the proposed catalytic mechanism. In addition, a third model called D-Gln-docked has been built from the coordinates obtained after docking a D-Gln residue in the active site of MurI by using a docking computational method. Starting from the different orientations of the ligand, classical molecular dynamics simulations have been carried out to investigate the binding interactions between D-Gln and the enzymatic residues in the active site of MurI, which are schematically represented in Figure 1.

We start by analyzing the results obtained with the D-Gln-X-ray model. Figure 2 compares the initial configuration with the position of the ligand in the active site of MurI obtained after 1.2 ns of SBMD (following 130 ps of heating and equilibration). Figure 2a, together with the initial distances shown in the last column of Table 1, indicate that Asn71 is the only enzymatic residue that forms an important interaction with D-Gln at the initial structure. Weaker interactions may be deduced from the distances between the main-chain ammonium group nitrogen of the ligand and both the main-chain oxygen of Gly177 and the side-chain Oδ1 atom of Asn71. As mentioned by Hwang et al.,[19] the observation of very few interactions between D-Gln and MurI in the crystallized structure is in agreement with its low inhibitory activity (KI = 50 mM). The comparison between the initial distances and the average distances calculated over 6000 saved configurations, and listed in the seventh column of Table 1, suggests that no new interactions are formed during the simulation. In the structures of the equilibrated system the hydrogen bond between the Oϵ1 atom of D-Gln and Asn71 is weaker than in the initial configuration. The relatively low occupancy, short average lifetime, and large number of times that this hydrogen bond is reformed agree with the longer interaction distance. On the contrary, the interactions between the main-chain amino group of the ligand and the enzyme are shorter in the structures generated during the SBMD simulations. Interestingly, these results

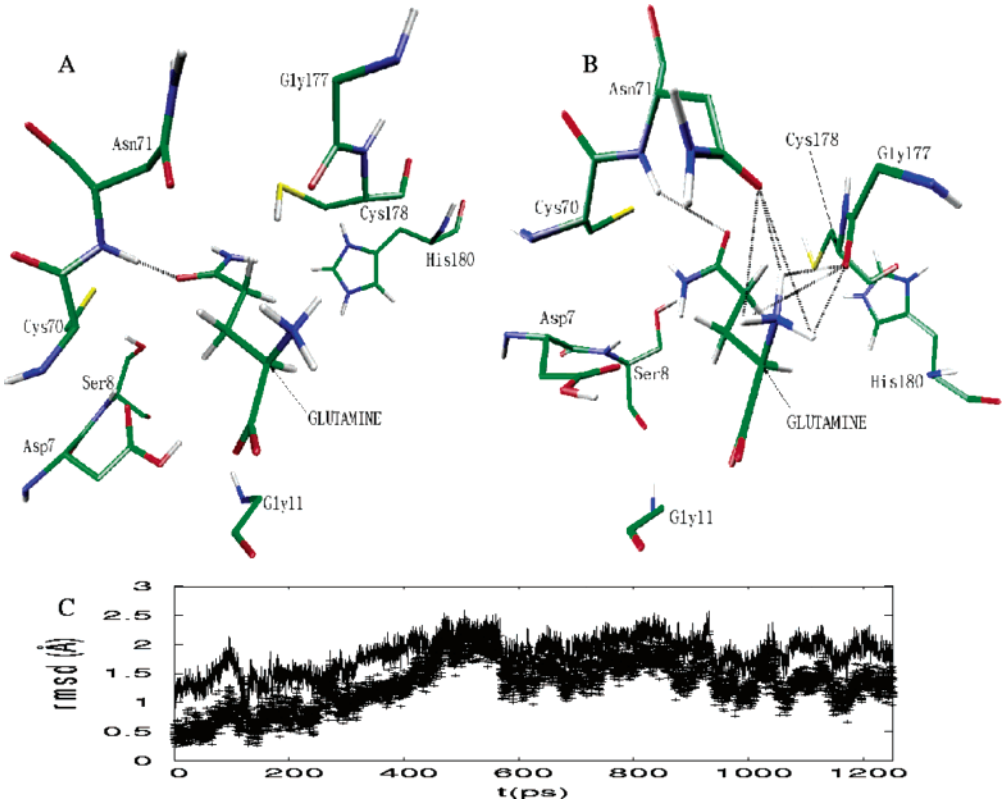

Figure 2. **(a)** Partial view of the active site of the D-Gln-X-ray model at the initial configuration. The shortest interactions between the ligand and the enzyme are marked with a dotted line. **(b)** Same as **(a)** at the final configuration of the 1.2 ns simulation. **(c)** Root-mean-square deviation (rmsd) of the ligand in the D-Gln-X-ray model as a function of the time along the sampling trajectory. The reference structure is the initial configuration (solid line) or the last configuration generated during the equilibration stage (crosses). In both cases, each frame has been reoriented in order to minimize the rmsd of the backbone atoms of the enzyme + ligand system with respect to the reference structure.

indicate that the D-Gln ligand remains in the flipped orientation found by Hwang et al.[19] despite being weakly bound in the active site of MurI.

To compare two different structures we have used the following strategy: First, we have reoriented the second structure in order to minimize the root-mean-square deviation (rmsd) of the backbone atoms of the enzyme + ligand system with respect to the corresponding atoms of the first structure; then, we have calculated the rmsd of just all the atoms of the ligand of the reoriented second structure with respect to the corresponding atoms of the first structure. So, Figure 2c shows the calculated rmsd of the ligand in the D-Gln-X-ray model along the 1.2 ns simulation using two different reference structures. The rmsd of the ligand with respect to both, the initial structure and the last structure generated during the equilibration stage, is small at the beginning of the trajectory and increases during the first 500 ps to reach a more stable behavior. The trends are almost parallel between the two calculated rmsds, which indicates that there is a very small difference between the two reference structures. Overall, the average rmsds of the ligand calculated over the trajectory are relatively small, with values of 1.83 and 1.31 Å with respect to the initial structure and the last configuration generated during the equilibration stage, respectively. These results are in agreement with the small deviation of the D-Gln orientation from the flipped configuration mentioned above. Thus, our simulation indicates that the relative orientation of D-Gln deduced from the X-ray experiment is stable, although weakly bound (see also the ligand-environment interaction energy section below), in the active site of MurI. Importantly, our results also indicate that this orientation is not suitable for the reaction. That is, the calculated average distances between the α-carbon of D-Gln and the sulfur atoms of the catalytic cysteines are larger than 7.0 Å.

Next, we analyze the results obtained with the D-Gln-modeled model. Figure 3 clearly indicates that the change from the initial to the final structures obtained with this model is larger than the one obtained with the D-Gln-X-ray model. At the initial configuration, the only short interaction between the ligand and the enzyme is the hydrogen bond between the Oτ2 atom of D-Gln and the protonated carboxylic group of Glu147 (see last column of Table 1). In addition, the protonated Cys178 forms a weak interaction with the other main-chain carboxylate oxygen of the ligand, and, like in the case of D-Gln in the flipped orientation (see above), there is a weak interaction between the NH3-group of D-Gln and the side chain of Asn71. These three interactions are maintained during the simulation of the equilibrated system (see the seventh column of Table 1), although the hydrogen bond distance between the ligand and Glu147 elongates, suggesting that this interaction is weakened. This is concomitant with the appearance of three new hydrogen bonds between D-Gln and the enzymatic residues. Specifically, the main-chain amino group of Thr179 interacts with the Oϵ1 atom of D-Gln, and the two main-chain carboxylate oxygens

Table 1. Important Hydrogen Bond Interactions between D-Glutamine and Enzymatic Residues for the Simulations of the Different Models Defined in the Text[a]

ligand atom	residue-atom	occu	time	events	dist	fluct	init
			D-Gln-X-ray				
Oϵ1	Asn71-HN	0.58	0.7	1106	2.41	0.45	1.65
NH3	Gly177-O	0.95	8.1	146	2.80	0.21	3.45
NH3	Asn71-Oδ1	0.88	2.6	420	2.86	0.25	4.18
			D-Gln-Modeled				
Oϵ1	Thr179-HN	0.84	4.4	240	2.17	0.61	6.18
O$_t$1	His180-Hϵ2	0.26	2.1	151	3.06	0.76	8.98
O$_t$1	Cys178-Hγ1	0.21	0.5	514	3.58	1.17	3.25
O$_t$2	His180-Hϵ2	0.89	3.3	333	1.93	0.40	6.95
O$_t$2	Glu147-Hϵ2	0.52	2.1	298	2.83	1.25	1.67
NH3	Asn71-Oδ1	0.75	1.9	503	3.06	0.51	3.67
			D-Gln-Docked				
Oϵ1	Asn71-HN	0.56	2.1	260	2.95	1.14	1.95
Oϵ1	Asn71-Hδ22	0.52	1.9	278	3.33	1.80	1.66
Oϵ1	Glu147-Hϵ2	0.26	1.5	176	3.16	0.86	4.90
O$_t$2	Tyr39-HN	0.96	5.4	178	1.96	0.21	2.02
O$_t$2	Gly40-HN	0.70	0.9	750	2.27	0.27	2.21
O$_t$2	Thr72-Hγ1	0.92	3.4	271	1.91	0.29	4.53
NH3	Val37-O	0.96	6.3	153	2.80	0.14	2.73

[a] For a given interaction, columns 4−9 show the following: hydrogen bond occupancy, average lifetime (in ps), number of times that the hydrogen bond is reformed (events), average interaction distance (in Å), root-mean-square (rms) fluctuations of the interaction distance (in Å), and hydrogen bond distance at the initial configuration (in Å). The criterion used to define the formation of a hydrogen bond is a distance smaller than 2.4 Å between the hydrogen and the acceptor atom. In the case of interactions between the amino group (NH3) of the ligand and the enzymatic residues, a hydrogen bond is considered to exist when any of the amino group hydrogens accomplishes the criterion explained above. In general, the interaction distance and its rms fluctuations refer to the distance between the hydrogen and the acceptor atom in the hydrogen bond, with the exception of the interactions involving the amino group (NH3) of the ligand, for which the distance between the donor and the acceptor atoms is given. Figure 1 indicates the meaning of the atom labels used in the table.

of the ligand become bound to His180. The short distances of these three hydrogen bonds agree well with the calculated occupancy, the average lifetime, and the number of events.

Figure 3c shows the rmsd of the ligand in the D-Gln-modeled model along the trajectory with respect to the initial structure and the last structure from the equilibration period. Similarly to the results obtained for the D-Gln-X-ray model, the rmsds at the beginning of the trajectory are small, and the parallelism of the two curves in Figure 3c suggests that the two reference states are quite similar. The D-Gln ligand slightly deviates from the modeled orientation during the first 500−600 ps, but at this point there is a jump in both rmsds, suggesting the occurrence of a significant conformational change. The comparison between parts a and b of Figure 3 highlights the movement of the main-chain atoms of D-Gln toward the contiguous residues Thr179-His180 to form interactions that were not present in the initial state. Consequently, the ligand moves far away from the Asp7-Ser8 residues and slightly from Glu147. The analysis of the evolution of the distance between these residues and D-Gln has given us a possible explanation for the sudden change of the rmsd value after 600 ps. Figure 3d summarizes these findings. At the beginning of the trajectory, the interaction found between the ligand and Glu147 in the initial configuration is maintained. However, His 180 gradually approaches to the Oτ2 atom of D-Gln and around the 500−600 ps region the interactions of the ligand with these two residues become competitive. After 700 ps and for ca. 400 ps, His 180 displaces Glu147, but the interaction with the latter is recovered after this period and stays in competition with the His180 interaction. Thus, there has probably been a change in the conformation of the ligand that allows these two interactions to occur simultaneously. In summary, the D-Gln molecule significantly moves from the position modeled by Hwang et al.[19] This is reflected by the higher values obtained with this model for the average rmsd of the ligand (2.79 and 1.62 Å, taking as reference the initial structure and the last structure of the equilibration period, respectively) in comparison with the D-Gln-X-ray model. In addition, as a consequence of the deviation of the ligand from the modeled position, which was suitable for reaction, its distance to the catalytic cysteines increases. The calculated average distance between the α-carbon and the sulfur atom of Cys70, which is proposed to abstract the α-proton, is 7.18 Å, 2.92 Å away from the modeled position, which suggests that the ensemble of equilibrated structures obtained for glutamine from the D-Gln-modeled model is not reactive.

The initial structure for the third model, the D-Gln-docked model, has been obtained from the analysis of the docked configurations obtained with 10 runs of the Lamarckian Genetic Algorithm implemented in AutoDock 3.0.[33] The configurations generated for the ligand were clustered using an rmsd tolerance of 0.5 Å. Then the clusters whose configurations were not suitable for catalysis were eliminated. Finally, the configuration with the lowest binding free energy in the most populated surviving cluster was selected as the initial structure for the D-Gln-docked model SBMD simulation (shown in Figure 4a). The distances given in the last column of Table 1 indicate that in this initial structure the shortest hydrogen bonds are formed between residue Asn71 and the Oϵ1 atom of D-Gln. The ligand is also bound by its carboxylate end to residues Tyr39 and Gly40, and there is a somewhat longer hydrogen bond between the NH3 group and Val37. In comparison to the relative orientation of D-Gln in the two previous models, the D-Gln-docked model resembles more the D-Gln-modeled system. However, docking has translated the ligand inside the active site in such a way that it interacts with residues not present in the close environment of the two previous models. During the simulation after the equilibration period, the hydrogen bond with Asn71 elongates (mainly due to a rotation of the ligand which can then connect through Oϵ1 with Glu147). At the carboxylate end, a new hydrogen bond is formed between the Oτ2 atom and residue Thr72 which presents the shortest distance and a high occupancy. Interestingly, the average value (5.18 Å) of the distance between the α-proton of D-Gln and the Sγ atom of Cys70 is quite shorter than the corresponding distance in the D-Gln-X-ray and D-Gln-modeled systems (8.03 and 7.20 Å, respectively). In addition, the Cα of D-Gln is closer to the two sulfur atoms of the

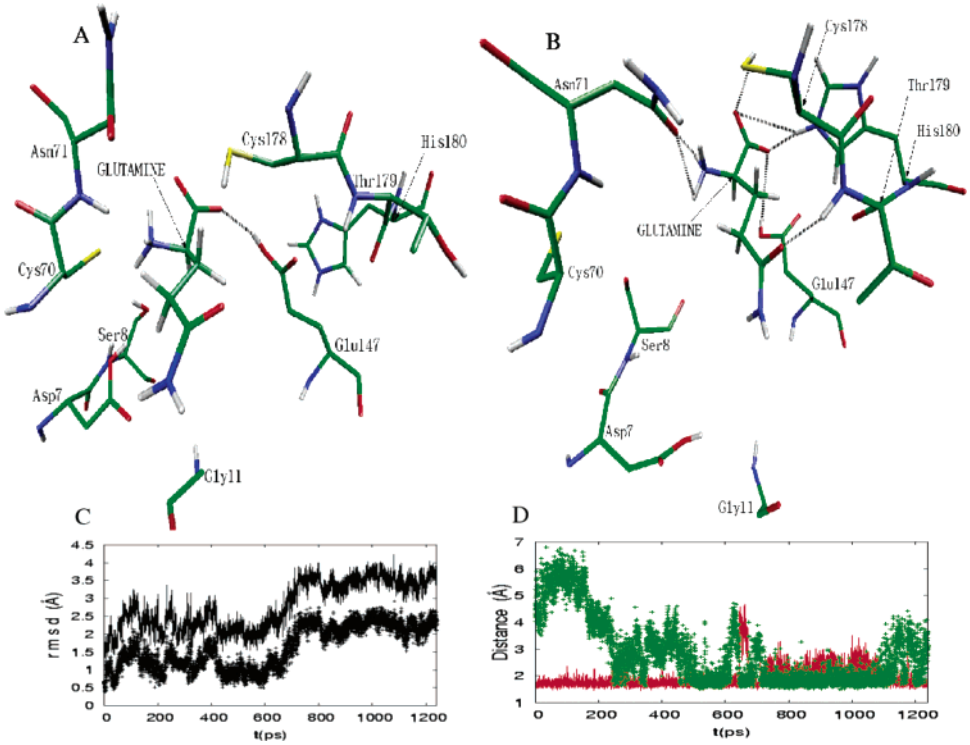

Figure 3. (a)−(c) Same as Figure 2(a)−(c) for the D-Gln-modeled model. (d) Interaction distances between the Hϵ2 atom of Glu147 (solid line, red) or the Hϵ2 atom of His180 (crosses, green) with the Oτ2 atom of glutamine along the sampling trajectory of the D-Gln-modeled model.

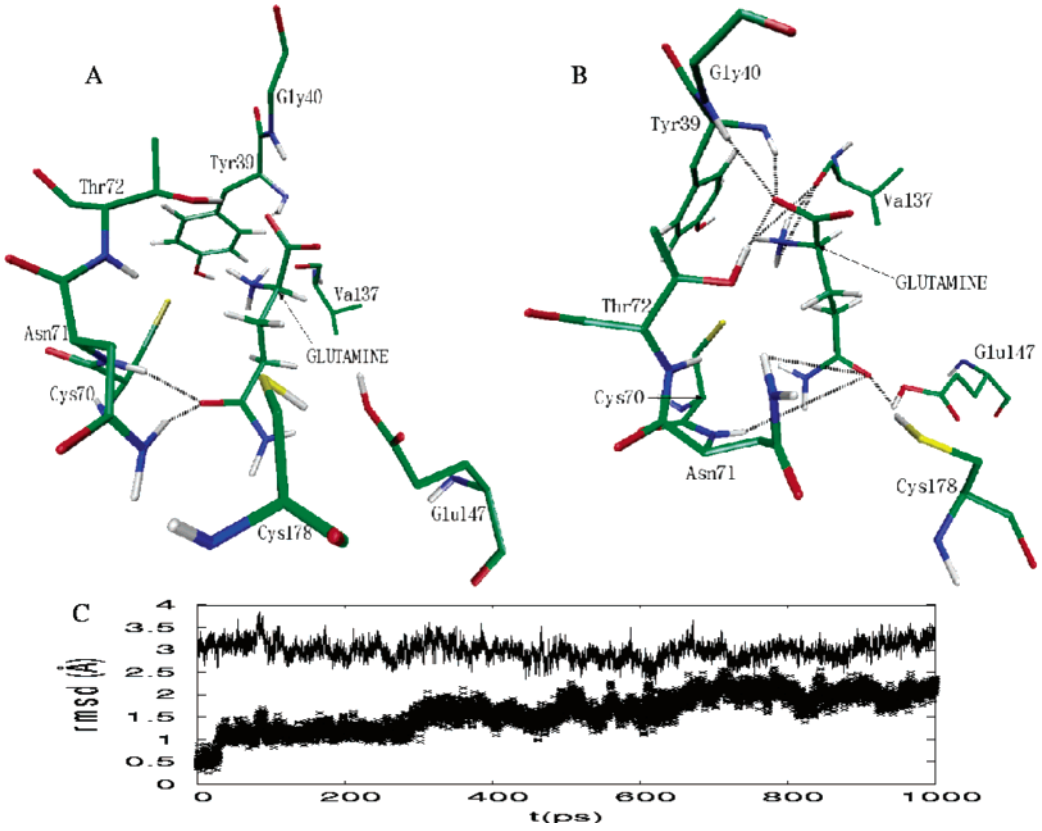

Figure 4. (a)−(c) Same as Figure 2(a)−(c) for the D-Gln-docked model.

catalytic cysteines (4.43 and 5.80 Å from Cys70 and Cys178, respectively) than in the D-Gln-modeled model, and both distances are shorter than the values observed by Hwang et al.[19] from their crystallographic studies on MurI (5.3 and 7.6 Å, respectively). These results indicate that the D-Gln inhibitor may also be found in a conformation similar to the one that would be reactive (in the case of D-Glu substrate) in the mechanism proposed by Glavas and Tanner.[17]

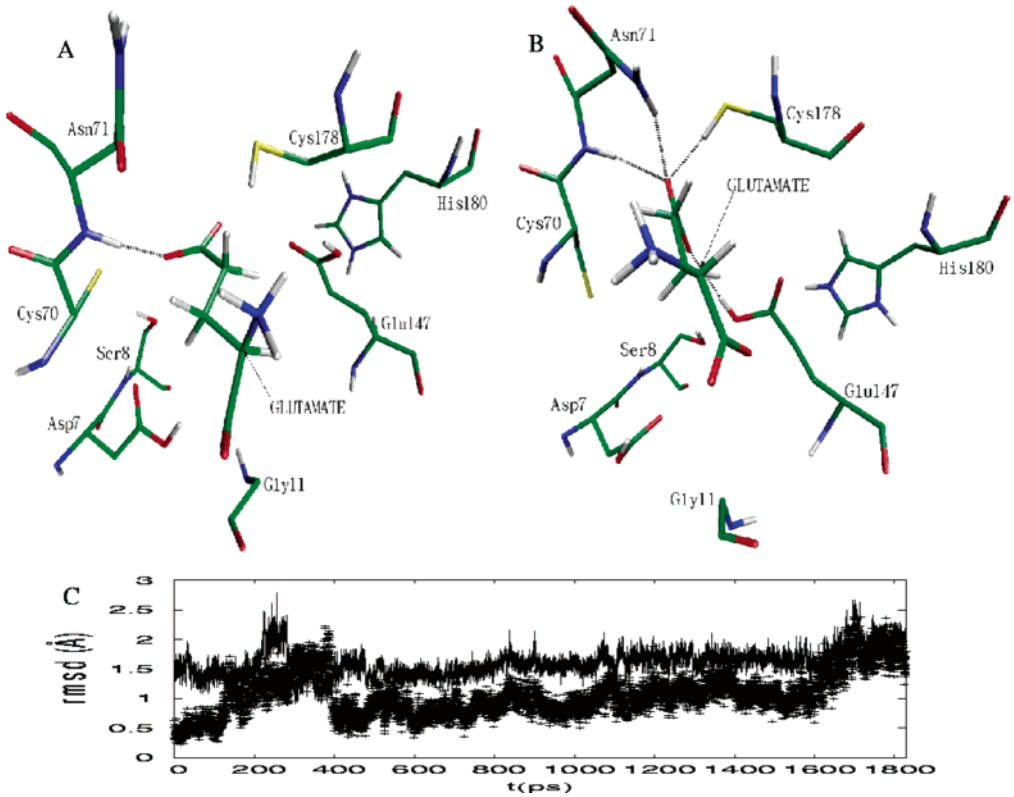

Figure 5. (a)−(c) Same as Figure 2(a)−(c) for the D-Glu-X-ray model.

The average rmsd of the ligand in the D-Gln-docked model with respect to the initial structure and calculated over the trajectory is rather big: 2.98 Å. This value shows that the D-Gln ligand has significantly moved from its initial location in the docked structure. The two rmsds calculated along the simulation steps and plotted in Figure 4c are clearly different. The rmsd value with respect to the initial docked structure is large but oscillates somewhat along the sampling stage, whereas the calculated rmsd with respect to the last structure of the equilibration stage experiments a significant increase along the simulation. These results indicate that the D-Gln ligand does not reach a stable position within the 1.0 ns time range, consequently with the lack of tight bindings to surrounding residues.

Binding of D-Glu in the Active Site of MurI. The different models of the D-Glu/*Aquifex pyrophilus* MurI complex are based on the same enzyme Cartesian coordinates used to build the D-Gln/*Aquifex pyrophilus* MurI models. However, for the D-Glu ligand we have taken the coordinates of the inhibitor D-Gln obtained from X-ray crystallography and the ones modeled by Hwang et al.,[19] and, in both cases, we have replaced the side chain group −NH2 of this molecule by a carboxylic oxygen to represent the carboxylate side-chain group of D-Glu. The resulting models are called D-Glu-X-ray and D-Glu-modeled, respectively, in this paper. We have followed the procedure indicated in the Methods section to prepare the initial structure for the simulation. In addition, a third model of the D-Glu/*Aquifex pyrophilus* MurI complex has been built using the coordinates obtained after docking a D-Glu molecule in the active site of MurI. This third model is called D-Glu-docked in this paper.

In Figure 5 the initial and the final configuration of the 1.8 ns SBMD simulation for the D-Glu-X-ray model can be compared. Like in the initial structure of the D-Gln-X-ray complex, only one significant ligand−enzyme interaction could be detected in the D-Glu-X-ray model (see Figure 5a and the last column in Table 2) corresponding to a short H-bond between Asn71 and the main-chain Oϵ1 atom of D-Glu. In addition, the D-Glu initial structure presents some other weaker substrate−enzyme interactions with Cys178, Glu147, and Gly177. From the average distance values included in the seventh column of Table 2 and the final configuration plotted in Figure 5b, it can be inferred that the D-Glu substrate modifies its location inside the MurI active center. After equilibration, the substrate tightens its interactions with the side chains of Asn71, Cys178, and Glu147 in addition to preserving, although somewhat longer, the initial Oϵ1-Asn71-NH hydrogen bond. Asn71 interacts now with the Oϵ1 atom of D-Glu also via its Hδ22, and the hydrogen bond with Cys178 has become shorter. However, the shortest hydrogen bond, with the highest occupancy, longest average lifetime, and smallest number of events (indicating that this hydrogen bond has not been broken and reformed often along the simulation), corresponds to the interaction between the main-chain Oϵ2 atom of D-Glu and Glu147. At this point, it is worth recalling that Glu147 (Glu152 in *L. fermenti*) has been proposed by Glavas and Tanner[17] to play an important role in substrate binding since the E152Q mutant showed only a modest decrease in the value of k_{cat}, whereas the value of K_M for D-Glu increased by 13-fold.

Table 2. Important Hydrogen Bond Interactions between D-Glutamate and Enzymatic Residues for the Simulations of the Different Models Defined in the Text[a]

ligand atom	residue-atom	occu	time	events	dist	fluct	init
			D-Glu-X-ray				
Oϵ1	Asn71-HN	0.96	5.8	304	1.98	0.21	1.65
Oϵ1	Asn71-Hδ22	0.93	3.1	553	2.01	0.25	5.30
Oϵ1	Cys178-Hγ1	0.37	0.4	1580	2.75	0.69	3.41
Oϵ2	Glu147-Hϵ2	0.98	24.8	72	1.80	0.25	3.83
NH3	Gly177-O	0.38	0.8	835	3.12	0.34	3.45
			D-Glu-Modeled				
Oϵ2	Asp7-Hδ2	1.00	412.5	3	1.68	0.11	5.68
Oϵ2	Gly11-HN	0.35	0.8	565	2.66	0.51	6.61
O$_t$1	Thr72-Hγ1	0.89	3.1	356	1.98	0.31	3.68
O$_t$2	Glu147-Hϵ2	0.92	11.3	101	1.84	0.40	1.62
O$_t$2	Cys178-Hγ1	0.48	0.7	882	2.67	0.75	2.94
O$_t$2	Thr72-Hγ1	0.38	0.8	619	2.53	0.43	5.57
NH3	Ser8-Oγ	0.84	1.6	647	2.95	0.20	6.36
NH3	Asp7-Oδ1	0.78	2.4	401	3.03	0.45	6.02
			D-Glu-Docked				
Oϵ1	Tyr39-HN	0.65	2.4	267	2.36	0.67	3.67
Oϵ1	Gly40-HN	0.77	9.3	82	2.32	0.76	2.22
Oϵ2	Thr72-Hγ1	0.63	39.2	16	3.10	1.87	3.21
Oϵ2	Thr114-Hγ1	0.78	65.3	12	2.63	1.68	4.04
O$_t$1	Asn71-Hδ22	0.48	1.5	323	2.48	0.57	5.52
O$_t$1	Thr72-HN	0.52	4.8	109	2.58	0.76	3.93
O$_t$1	Thr72-Hγ1	0.35	6.5	54	3.63	1.40	5.51
O$_t$2	Asn71-Hδ22	0.46	1.2	384	2.74	0.77	7.63

[a] See Table 1 for details of the content of each column.

All the changes in the D-Glu arrangement inside the MurI active site in the D-Glu-X-ray model indicate that the substrate modifies its hydrogen bond network relative to the initial structure. Despite this, the calculated average rmsd (1.61 Å) of D-Glu with respect to the initial structure is small; in fact, even smaller than the corresponding value for D-Gln (1.83 Å). The average rmsd for D-Glu with respect to the last structure of the equilibration stage is 1.06 Å (compared to 1.31 Å for D-Gln). Figure 5c shows the evolution of the rmsd of the substrate ligand with respect to the two different reference structures as a function of the simulation time. It can be seen that no significant structural instability appears. To understand these low average rmsds we have superimposed the initial and the final structure of the simulation. The comparison of the two structures indicates that the formation of new interactions is mainly due to movements of the enzyme residues side chains. This more stable behavior of the D-Glu ligand along the simulation explains the smaller value obtained for the average rmsd. The same trends are followed by the rmsd of the ligand referred to the last structure of the equilibration stage. In any case, our results about the relocation of the substrate ligand inside the active site do not significantly change the flipped orientation found by Hwang et al.[19] for D-Gln, and used by us to build the D-Glu-X-ray model. This is confirmed by the long average distances of 7.10 and 6.62 Å between the α-carbon of D-Glu and the Sγ atom of Cys70 and Cys178, respectively. Thus, our results show that the D-Glu substrate can be bound inside the active site of MurI in a stable conformation which, however, is not adequate to initiate the first chemical step proposed in Tanner's mechanism.[17]

The second model built to study D-Glu binding in MurI has been called D-Glu-modeled. In Figure 6 the initial and final structures corresponding to the 1.2 ns SBMD simulation carried out on this D-Glu-modeled system have been plotted. Like in the D-Gln-modeled case, the only existing interaction at the initial state between the ligand and the enzyme corresponds to a short hydrogen bond between the Oι2 atom of D-Glu and the protonated carboxylic group of Glu147 (see the last column of Table 2). In addition, the ligand forms two other weaker interactions with the enzyme: a long hydrogen bond between the same Oι2 atom of D-Glu and the protonated Cys178 and another long hydrogen bond between the other main-chain carboxylate oxygen of the ligand and Thr72. The average distances presented in Table 2 show that these three interactions are maintained along the simulation of the equilibrated system although with some changes: the hydrogen bond between the substrate and Glu147 slightly elongates, whereas the hydrogen bond with Thr72 clearly shortens. In addition, five new interactions are formed between the substrate and the enzyme once the system has been equilibrated. From Figure 6b and the average distances given in Table 2, it can be observed that the D-Glu substrate is hydrogen-bonded to the enzyme by the positively charged ammonium group (which is stabilized by Ser8 and Asp7) and by the two negatively charged carboxylate groups (the main-chain carboxylate interacts with Glu147, Cys178, and also Thr72, whereas the side-chain carboxylate interacts with Asp7 and Gly11). The shortest hydrogen bond in the ensemble of equilibrated structures of the D-Glu-modeled system corresponds to the interaction between Hδ2 of Asp7 and Oϵ2 of D-Glu. This hydrogen bond has an occupancy of 1.00, a very long average lifetime, very small fluctuations, and in only 3 events along the simulation it is broken and reformed. All this three observations are clear proofs of its high stability. As indicated above, the mutagenesis studies carried out by Glavas and Tanner[17] have supported the important role in catalysis of Asp7 (Asp10 in *L. fermenti*).

In agreement with the large differences between the initial and average distance values for the interactions listed in Table 2, Figure 6c indicates that the D-Glu ligand in the D-Glu-modeled system has clearly changed its relative orientation in the active site with respect to the initial coordinates of the D-Glu-modeled model. The average rmsd of the ligand with respect to the initial structure is 2.81 Å, clearly larger than the corresponding values obtained in the D-Glu-X-ray model and in the D-Gln-X-ray one. In addition, the differences observed between the calculated rmsds of the ligand, one with respect to the initial structure and the other with respect to the last structure of the equilibration stage, reflect that in this case the two reference states are not alike. The average rmsd with respect to the last structure of the equilibration stage takes a value of only 1.09 Å, corroborating the tight binding of the D-Glu ligand in this model. Interestingly, the calculated average distance between the α-carbon and the residue proposed to abstract the α-proton in the first chemical step of Tanner's mechanism[17] (Cys70) is 4.62 Å, a smaller value than the one calculated for the

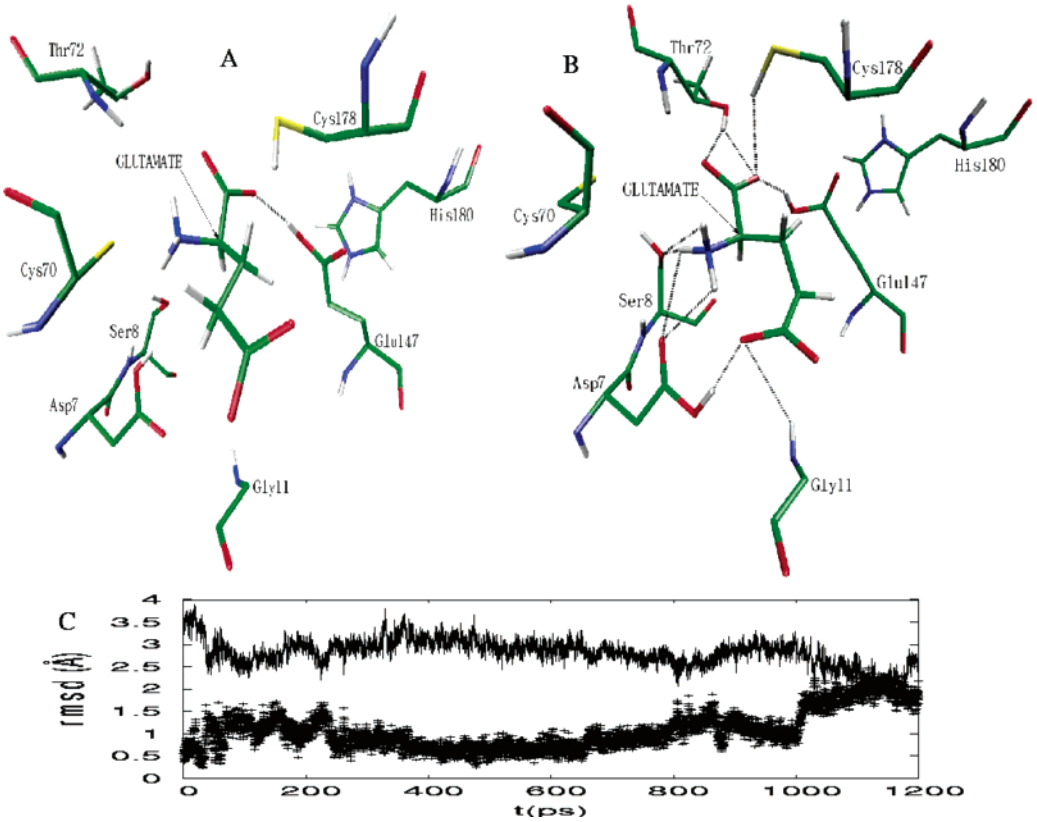

Figure 6. (a)−(c) Same as Figure 2(a)−(c) for the D-Glu-modeled model.

D-Glu-X-ray model. This result suggests that the equilibrated structure for the D-Glu substrate in the D-Glu-modeled system may be a good starting point for the study of the reactivity of MurI.

The initial structure for the third model of binding of D-Glu in the active site of MurI (D-Glu-docked) has been obtained following the flexible docking protocol detailed in the Methods section. In accordance with the three selection criteria used for the D-Gln ligand, one docked structure (plotted in Figure 7a) was selected to initiate the SBMD simulation. In this structure the D-Glu ligand adopts a relative orientation to the enzyme rather similar to the one in the D-Glu-X-ray model, that is, flipped 180° with respect to the substrate location in the D-Glu-modeled system. However, the center of mass of D-Glu is translated with respect to its position in the previous two models. As a consequence, the Cα-Sγ distance is 4.17 Å for Cys70. This distance is clearly shorter than in the initial structure of the D-Glu-X-ray model and even shorter than in the D-Glu-modeled system initial structure. In addition, in Table 2 (last column) it can be observed that in this initial configuration the ligand forms a hydrogen bond with Gly40 and two other rather longer hydrogen bonds with Thr72 and Tyr39. These are maintained along the simulation in addition to some other hydrogen bonds which are newly formed. All these interactions retain the substrate in a rather stable conformation bound by the two negatively charged carboxylate ends to residues Gly40, Tyr39, Thr114, and Thr72 at one side and to residues Asn71 and Thr72 at the other side (see Figure 7b). In any case, the rather long average distances of these hydrogen bonds, their large fluctuations, along with the low occupancies indicate that D-Glu is not tightly bound in the D-Glu-docked model. Interestingly, two of the new residues which enter the scene (Tyr39, and Thr114) are strictly conserved, and they have been proposed as candidates for the residues of glutamate racemase that are thought to stabilize the anionic intermediate by hydrogen bonding to the carboxylate group.

The rmsds (in Figure 7c) of the ligand in the D-Glu-docked model with respect to both, the initial structure and the last structure generated during the equilibration stage, increase during the first 500 ps to reach a more or less stable behavior. The trends are almost parallel between the two calculated rmsds, which indicates that there is not much difference between the two reference states. Overall, the average rmsds of the ligand calculated over the trajectory are rather high, with values of 3.45 and 2.32 Å obtained with respect to the initial structure and with respect to the last structure after the equilibration stage, respectively. These results are in agreement with the weak binding of the substrate observed in this model and with the changes in its conformation, mainly due to a rotation movement of the ligand around itself that takes place along the simulation steps. However despite being weakly bound, the distance between the Cα of the ligand and the Sγ of Cys70 (4.02 Å) indicates that the ensemble of the equilibrated structures is suitable for reaction.

Finally, we have lengthened the SBMD simulation time for the D-Glu-X-ray (up to 2528 ps) and D-Glu-modeled (up to 2236 ps) models to test the convergence of the results. As shown in the Supporting Information (see Figures 3−21 and Tables 6−16), no significant changes in the main MurI-substrate interactions appear at longer simulation times.

Ligand-Environment Interaction Energy. We have also calculated the electrostatic component of the interaction energy (ΔE_{SE}) between the ligand and the enzyme-aqueous

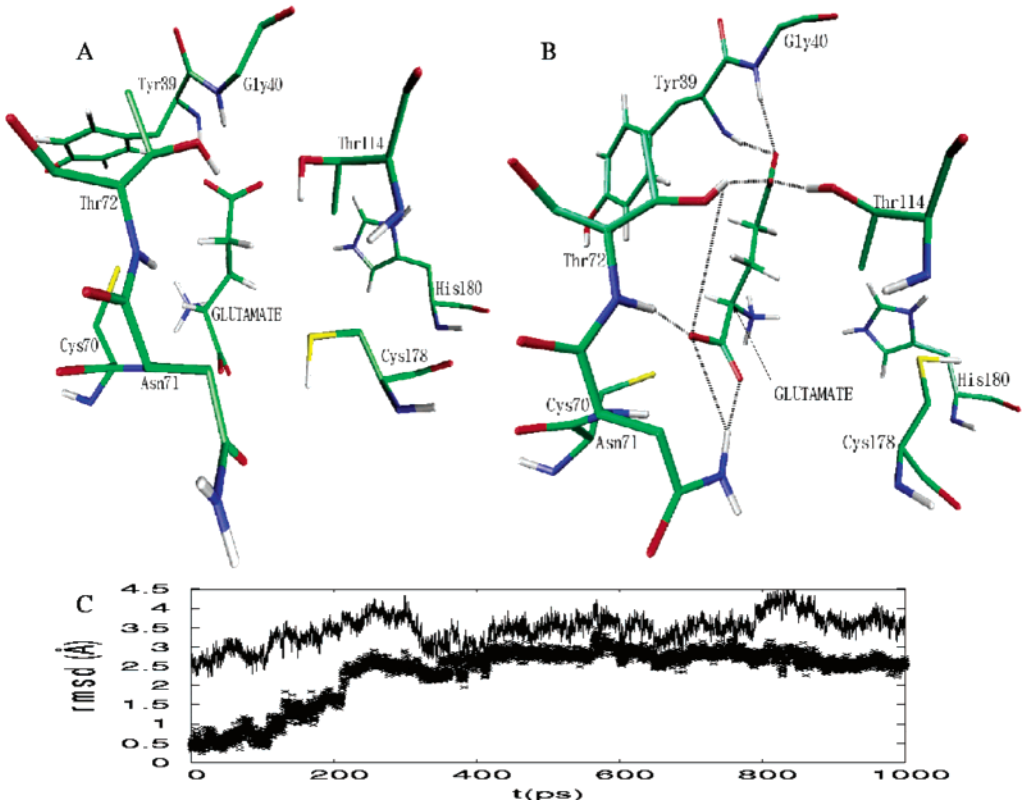

Figure 7. (a)−(c) Same as Figure 2(a)−(c) for the D-Glu-docked model.

Table 3. Electrostatic Component of the Ligand-Environment Interaction Energy and Its Decomposition in Different Terms[a]

model	ΔE_{SE}	ΔE_{perm}	ΔE_{pol}	ΔE_{stab}	ΔE_{dist}
D-Gln-X-ray	−106.69	−96.35	−10.34	−20.29	9.95
D-Gln-modeled	−114.92	−101.59	−13.33	−26.06	12.73
D-Glu-X-ray	−216.11	−202.65	−13.46	−26.39	12.93
D-Glu-modeled	−130.49	−124.75	−5.74	−11.22	5.48

[a]See text. All the energies are given in kcal/mol.

environment. First, the whole system is divided in a quantum mechanical (QM) subsystem (the ligand) and a molecular mechanical (MM) subsystem (the enzyme + aqueous environment). Then that electrostatic component is defined[34,35] as the difference between the energy of the ligand inside the enzyme + aqueous environment and that in the gas phase. ΔE_{SE} can be decomposed into the interaction energy between the unpolarized ligand and the environment (the permanent interaction energy, ΔE_{perm}) and the polarization energy of the ligand due to the environment (ΔE_{pol}). In turn, ΔE_{pol} may be further decomposed into a polarization stabilization term (ΔE_{stab}) and a ligand electronic distortion term (ΔE_{dist}).

For several models, and starting from the corresponding previously equilibrated systems, the energies have been obtained after averaging 10 ps of a SBMD simulation at 300 K on a QM/MM potential energy surface. The QM subsystem corresponding to the ligand (D-glutamine or D-glutamate) was represented by the AM1 semiempirical molecular orbital method.[36] The results are shown in Table 3. It can be seen that D-glutamate is clearly tighter bound to the enzyme than D-glutamine, specially in the D-Glu-X-ray model. In all cases the main contribution comes from the permanent interaction energy, although the polarization energy is also favorable and significant.

Conclusions

The active site of glutamate racemase from *Aquifex pyrophilus* contains many charged and polar residues. As a consequence, many ligand (D-glutamine or D-glutamate)−enzyme interactions can exist, making several binding modes possible. When the ligand is D-glutamine, our molecular dynamics simulations reveal three very different stable conformations of the inhibitor. One of them corresponds to the X-ray structure determined by Hwang et al.,[19] in which the α-carbon of D-glutamine is quite far from the two catalytic cysteines, confirming the experimental results. In the second conformation, derived from the structure modeled by Hwang et al.,[19] the α-carbon is not close to the two cysteines either. Only in a third conformation D-glutamine would be ready to initiate the reactive mechanism proposed by Glavas and Tanner[17] if it could behave as a substrate. In turn, at least three binding modes are possible for the substrate D-glutamate. In two of them D-glutamate is tightly bound (clearly more than D-glutamine) in the active site. One of these conformations comes from the X-ray structure determined for D-glutamine, whereas the other is related to the structure modeled for D-glutamine. In this second conformation the α-carbon is close to the two thiol groups of Cys70 and Cys178, making possible the deprotonation/reprotonation mechanism proposed by Glavas and Tanner[17] for the racemization of D-glutamate.

The existence of multiple modes of binding of the inhibitor D-glutamine and the substrate D-glutamate into the active site

of glutamate racemase might explain the apparent and surprising disagreement between the position and orientation of the inhibitor, inferred from X-ray crystallography data, and the expected position and orientation of the substrate, derived from the reaction mechanism proposed by Glavas and Tanner.[17] At this point, it has to be noted that accurate and expensive free energy calculations would be needed in order to determine the relative binding free energies of the different binding modes. However, the less costly molecular dynamics simulations of equilibrated complexes carried out in this paper are enough to provide an important structural information which shows the multiplicity of binding modes.

The initial coordinates for the theoretical study of the kinetics and mechanism of an enzymatic reaction are usually taken from a crystal structure of the enzyme complexed with a suitable inhibitor. However, in the present case, the unexpected features of the X-ray structure determined for D-glutamine prevents its use as an appropriate starting point for any reactivity study. Then, although we are rather interested in the kinetics of the deprotonation/reprotonation steps of D-glutamate, we have been forced to undertake the molecular dynamics simulation presented here. We think that our structural results provide reasonable starting points for the study of the reaction mechanism of glutamate racemase, which is already in progress in our laboratory. In any case, we think that, as already stated by Möbitz and Bruice,[37] the observation that D-glutamate can be accommodated in the active site of glutamate racemase according to several competitive binding modes, not all of them adequate for the racemization reaction, can have clear consequences on the kinetics of interconversion of glutamate enantiomers. As a matter of fact, the k_{cat} values of the glutamate racemization ($0.25\ s^{-1}$ for the Aquifex pyrophilus variant[38]) lies on the low range of k_{cat} values of enzymatic reactions. The biological reasons for favoring the presence of nonproductive enzyme−substrate complexes are at this stage unclear.

Acknowledgment. We are grateful for financial support from the Spanish "Ministerio de Ciencia y Tecnología" and the "Fondo Europeo de Desarrollo Regional" through Project No. BQU2002-0031 and the use of computational facilities of the CESCA.

Supporting Information Available: Parameters for the GB-MV2 method, molecular mechanics parameters for a deprotonated cysteine, SBMD simulation results with a sphere of 30 Å to define the reaction zone for the D-Glu-modeled system, and SBMD simulation results at longer times for the D-Glu-X-ray and D-Glu-modeled models. This material is available free of charge via the Internet at http://pubs.acs.org.

References

(1) Van Heijenoort, J. In *Escherichia coli and Salmonella*; Neidhart, F. C., Curtis, R., III, Ingraham, J. L., Lin, E. C. C., Low, K. B., Magasanik, B., Resnikoff, W. S., Riley, M., Schaechter, M., Umbarger, H. E., Eds.; American Society for Microbiology: Wahington, DC, 1996; p 1025.

(2) Ashiuchi, M.; Yoshimura, T.; Kitamura, T.; Kawata, Y.; Nagai, J.; Gorlatov, S.; Esaki, N.; Soda, K. *J. Biochemistry* **1995**, *117*, 495.

(3) Ashiuchi, M.; Kuwana, E.; Yamamoto, T.; Komatsu, K.; Misono, H. *J. Biol. Chem.* **2002**, *277*, 39070.

(4) Glavas, S.; Tanner, M. E. *Biochemistry* **1999**, *38*, 4106.

(5) de Dios, A.; Prieto, L.; Martín, J. A.; Rubio, A.; Ezquerra, J.; Tebbe, M.; López de Uralde, B.; Martín, J.; Sánchez, A.; LeTourneau, D., L.; McGee, J. E.; Boylan, C.; Parr, T., R., Jr.; Smith, M. C. *J. Med. Chem.* **2002**, *45*, 4559.

(6) Chu, D. T. W.; Plattner, J. J.; Katz, L. *J. Med. Chem.* **1996**, *39*, 3853.

(7) Gale, E. F.; Cundliffe, E.; Reynolds, P. E.; Richmond, M. H.; Waring, M. J. *The Molecular Basis of Antibiotic Action*, 2nd ed.; Wiley and Sons: London, 1981.

(8) Davis, J. *Science* **1994**, *264*, 375.

(9) Travis, J. *Science* **1994**, *264*, 360.

(10) Tanner, M. E.; Kenyon, G. L. In *Comprehensive Biological Catalysis*; Sinnott, M., Ed.; Academic Press: San Diego, 1998; p 7.

(11) Gerlt, J. A.; Kenyon, G. L.; Kozarich, J. W.; Neidhart, D. J.; Petsko, G. A.; Powers, B. M. *Curr. Opin. Struct. Biol.* **1992**, *2*, 736.

(12) Yamauchi, T.; Choi, S.-Y.; Okada, H.; Yohda, M.; Kumagai, H.; Esaki, N.; Soda, K. *J. Biol. Chem.* **1992**, *267*, 18361.

(13) Tanner, M. E.; Gallo, K. A.; Knowles, J. R. *Biochemistry* **1993**, *32*, 3998.

(14) Ho, H.-T.; Falk, P. J.; Ervin, K. M.; Krishnan, B. S.; Discotto, L. F.; Dougherty, T. J.; Pucci, M. J. *Biochemistry* **1995**, *34*, 2464.

(15) Doublet, P.; Van Heijenoort, J.; Mengin-Lecreulx, D. *Microb. Drug. Resist.* **1996**, *2*, 43.

(16) Tanner, M. E.; Miao, S. *Tetrahedron Lett.* **1994**, *35*, 4073.

(17) Glavas, S.; Tanner, M. E. *Biochemistry* **2001**, *40*, 6199.

(18) Tanner, M. E. *Acc. Chem. Res.* **2002**, *35*, 237.

(19) Hwang, K. Y.; Cho, C.-S.; Kim, S. S.; Sung, H.-C.; Yu, Y. G.; Cho, Y. *Nat. Struct. Biol.* **1999**, *6*, 422.

(20) Wiseman, J. S.; Nichols, J. S. *J. Biol. Chem.* **1984**, *259*, 8907.

(21) Higgins, W.; Tardif, C.; Richaud, C.; Krivanek, M. A.; Cardin, A. *Eur. J. Biochem.* **1989**, *186*, 137.

(22) Cirilli, M.; Zheng, R.; Scapin, G.; Blanchard, J. S. *Biochemistry* **1998**, *37*, 16452.

(23) Cho, Y., personal communication.

(24) Brooks, B. R.; Bruccoleri, R. E.; Olafson, B. D.; States, D. J.; Swaminathan, S.; Karplus, M. *J. Comput. Chem.* **1983**, *4*, 187.

(25) Lee, S. M.; Feig, M.; Salsbury, R., Freedie, J. R.; Brooks, C. L., III *J. Comput. Chem.* **2003**, *24*, 1348.

(26) Brooks, C. L., III; Karplus, M. *J. Chem. Phys.* **1983**, *79*, 6312.

(27) Brooks, C. L., III; Karplus, M. *J. Mol. Biol.* **1989**, *208*, 159.

(28) Mackerell, J., A. D.; Bashford, D.; Bellot, M.; Dunbrack, J., R. L.; Evanseck, J. D.; Field, M. J.; Fischer, S.; Gao, J.; Guo, H.; Ha, S.; Joseph-McCarthy, D.; Kuchnir, L.; Kuczera, K.; Lau, F. T. K.; Mattos, C.; Michnick, S.; Ngo, T.; Nguyen, D. T.; Prodhom, B.; Reiher, I., W. E:; Roux, B.; Schlenckrich, M.; Smith, J. C.; Stote, R.; Straub, J.; Watanabe, M.; Wiorkiewicz-Kuczera, J.; Yin, D.; Karplus, M. *J. Phys. Chem. B* **1998**, *102*, 3586.

(29) Jorgensen, W. L.; Chandrasekhar, J.; Madura, J. D.; Impey, R. W.; Klein, M. L. *J. Chem. Phys.* **1983**, *79*, 926.

(30) Rychaert, J. P.; Cicotti, G.; Berendsen, H. J. C. *J. Comput. Phys.* **1977**, *23*, 327.

(31) http://www.scripts.edu/pub/olson-web/dock/autodock/.

(32) Morris, G. M.; Goodsell, D. S.; Huey, R.; Olson, A. J. *J. Comput.-Aided Mol. Des.* **1996**, *10*, 293.

(33) Morris, G. M.; Goodsell, D. S.; Halliday, R. S.; Huey, R.; Hart, W. E.; Belew, R. K.; Olson, A. J. *J. Comput. Chem.* **1998**, *19*, 1639.

(34) Gao, J.; Xia, X. *Science* **1992**, *258*, 613.

(35) Garcia-Viloca, M.; Truhlar G., D.; Gao, J. *J. Mol. Biol.* **2003**, *327*, 549.

(36) Dewar, M. J. S.; Zoebisch, E. G.; Healy, E. F.; Stewart, J. J. P. *J. Am. Chem. Soc.* **1985**, *107*, 3902.

(37) Möbitz, H.; Bruice, T. C. *Biochemistry* **2004**, *43*, 9685.

(38) Bae, H.-S.; Hong, S.-P.; Lee, S.-G.; Kwak, M.-S.; Esaki, N.; Sung, M.-H. *J. Mol. Catal. B* **2002**, *17*, 223.

CT049881G